Conference on Modelling Fluid Flow (CMFF'22)
The 18th International Conference on Fluid Flow Technologies
Budapest, Hungary, August 30-September 2, 2022

1D THERMAL MODELLING OF A WHEEL BEARING TO INVESTIGATE ENERGY LOSSES

Márton KERÉNYI[1], István GORICSÁN[2], Thomas PITOUR[3]

[1] Corresponding Author. Thermo- /Energy Management Development, AUDI HUNGARIA Zrt G/GF-1, Audi Hungária út 1., H-9027 Győr, Hungary. E-mail: marton.kerenyi@audi.hu
[2] Thermo- /Energy Management Development, AUDI HUNGARIA Zrt G/GF-1. E-mail: istvan.goricsan@audi.hu
[3] Energiemanagement, AUDI AG I/EG-31, Auto-Union-Straße AUDI AG 1., 85057 Ingolstadt, Germany. E-mail: thomas.pitour@audi.de

ABSTRACT

This paper presents the 1D thermal multi-mass (TMM) simulation of a wheel bearing in order to estimate how the component temperatures affect the energy loss during the Worldwide Harmonized Light Vehicles Test Cycle (WLTC). The simulation model was developed in *MATLAB/Simulink* on the basis of the conductive and convective heat transfer equations.

The ambient air and bearing components are represented by 7 simplified thermal mass points. The physical quantities necessary to create these points such as area, mass and material of the components were taken from the bearing's 3D computer model. The heat transfer between the individual masses can be determined by setting different values of heat transfer coefficients. In this way it can be observed how much thermal insulation and proper material selection can improve the energy efficiency. The simulation model was created with speed, stability and robustness in mind in order to allow a level of accuracy that meets industrial and scientific expectations.

In order to validate the model, the simulation results were compared to experimental data. A case study with different heat transfer parameters was concluded to quantify the effect of insulation and so, the energy saving potential.

Keywords: 1D simulation, Heat transfer, Insulation, Thermal mass model, Wheel bearing, WLTP driving cycle

NOMENCLATURE

$\dot{Q}$	$[W]$	heat transfer rate
A	$[m^2]$	area
D	$[-]$	relative uncertainty
$FACn$	$[-]$	factor of n observations
FB	$[-]$	fractional bias
HR	$[-]$	hit rate
M_f	$[Nm]$	friction moment
MG	$[-]$	geometric mean
$NMSE$	$[-]$	normalised mean square error
O_i	$[-]$	observation point
P_f	$[W]$	friction power
P_i	$[-]$	prediction point
Q_0	$[kJ]$	initial heat energy
R_th	$[K/W]$	thermal resistance
T	$[K]$	temperature
T_0	$[K]$	initial temperature
V	$[m^3]$	volume
VG	$[-]$	geometric variance
W	$[-]$	absolute uncertainty
c_p	$[kJ/kgK]$	constant pressure specific heat
m	$[kg]$	mass
n	$[1/min]$	rotation speed
α	$[W/m^2K]$	convective heat transfer coefficient
δ	$[m]$	wall thickness
λ	$[W/mK]$	thermal conductivity
ω	$[rad/s]$	angular velocity

1. INTRODUCTION

During normal operation of a road vehicle, unavoidable resistances are being encountered. These resistant forces, such as the aerodynamic drag, gravitational forces due to road gradient, inertial forces during acceleration and rolling resistance all appear in the form of energy loss [1, 2]. The necessity of the reduction of such forces are becoming more significant with the decreasing amount of allowed tank-to-wheel CO_2 emissions and so, fuel consumption imposed by regulations. In the EU, the regulation thresholds are standardised on the basis of driving cycle tests, such as the currently used Worldwide Harmonised Light Vehicles Test Cycle (WLTC). [3]

One of the main causes of wasted energy is friction between mechanical parts that are in physical contact with each other and experience relative displacement. Such can be observed inside the wheel bearing assembly. The power dissipation in the bearing increases with decreasing component temperature which is primarily influenced by the friction heat

and the thermal properties of the materials.[4]

The purpose of this paper is to present a 1D thermal multi-mass (TMM) simulation that can be used to measure the power dissipation of a wheel bearing during a driving cycle. The parts of the bearing and the relevant nearby components are handled as thermal mass points between which heat transfer connection is built using *Fourier's law* for conduction and *Newton's law of cooling* for convection. In the first section, the theoretical considerations behind the model is introduced, then the results of the simulation cycles are compared to the corresponding measurements using statistical metrics as a validation method. In the last section, the different insulation methods are presented and their impact on energy loss due to friction.

2. CONSTRUCTION OF THE MODEL

This section introduces the mathematical and physical methods along which the bearing assembly is modeled as a 1D thermal system.

2.1. Heat generation inside the bearing

The simulation model is based on a double row deep groove ball bearing. Ball bearings are widely used for places where low energy losses due to friction is prioritised. Still, frictional losses cannot be avoided entirely. During operation, relative motion of the inner and outer rings causes the balls to rotate between them. Without radial load on the bearing, the balls' connection with the rings is at a point or along a line. In the presence of radial load, the contact surface transforms into a face as a result of the plastic deformation of the rolling elements caused by stresses according to the Hertzian contact theory [5]. The deformation brings along the increment of the rolling resistance thus more kinetic energy turns into heat. The net effect of friction also appear as a force that creates a counter torque opposing the drive torque.

The other source of the frictional torque is viscous friction. As it is pointed out in Yang and Jeng's work [6], the friction force between the rotating components and the lubricant oil increases with increasing oil viscosity. However, oil viscosity decreases as the temperature goes up [7], proportionally with the speed of the shaft. These relations can be seen in Figure 1 based on measurement data. The exact temperature values in *Kelvin* have been normalised with a constant temperature also measured in *Kelvin*.

With the M_f friction moment at different temperature levels and ω angular velocities, the P_f friction power can be calculated in kW according to Eqn. (1).

$$P_\mathrm{f} = M_\mathrm{f} \cdot \omega \tag{1}$$

2.2. Modeling the heat transfer

The generated heat between the inner and outer rings can dissipate in the form of radiation, conduction and convection [8]. By reason of the relative low

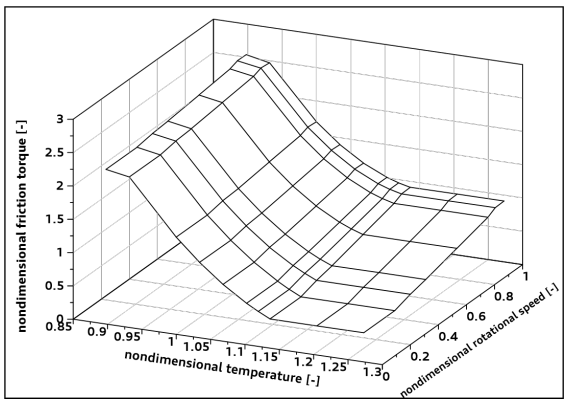

Figure 1. Experimentally determined relation between the friction moment versus temperature and shaft rotation speed

level of operating temperature, propagation through radiation has not been considered in the paper. The heat is transferred to the neighbouring parts like the wheel hub, inner ring and outer ring based upon the ratio of the surfaces that participate in the heat conduction. Because the outer ring has significantly larger connecting surface to the ambient air compared to the other components, convective heat transfer is only modeled between them. The first stage of the heat transfer process is shown in Figure 2.

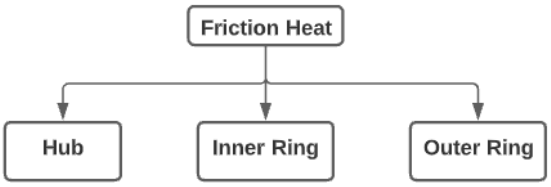

Figure 2. The distribution of friction heat from the source

The friction heat between the rings is transferred to the wheel hub and to both rings via conduction. The balls were considered as parts of the outer ring and in the model they form a single part with their masses combined. A similar method is used by J.Takabi and M. M. Khonsari in their model regarding the mass of the cage and balls [7]. According to our method the cage around the balls was not considered due to the low mass and low heat storage capability. The heat propagation is distributed further in Figure 3.

The inner ring is pressed onto the wheel hub and supported by the shoulder of the driven shaft so there are two surfaces and directions where heat can be transferred. The hub is heated directly by the source of the heat and by the inner ring. The brake disc is supported by an annular surface of the hub through which conduction can take place. The hub is fixed on the driven shaft by a spline connection and by an end plate. Both the net surface of the spline teeth and the annular surface of the plate were considered in

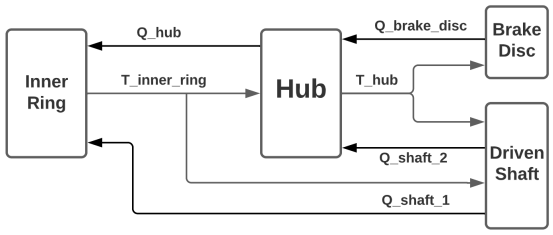

Figure 3. Heat distribution from the inner ring with negative energy feedback

the calculations. It needs to be mentioned that due to the relative large mass of the brake disc and shaft, their initial temperature is modeled so that they remain constant in time, unaffected by the heat transfer process. The negative feedback contains the amount of heat in kJ that the hotter object passes on to the part that it is in connection with. The heat flow at the outer ring is modeled in Figure 4.

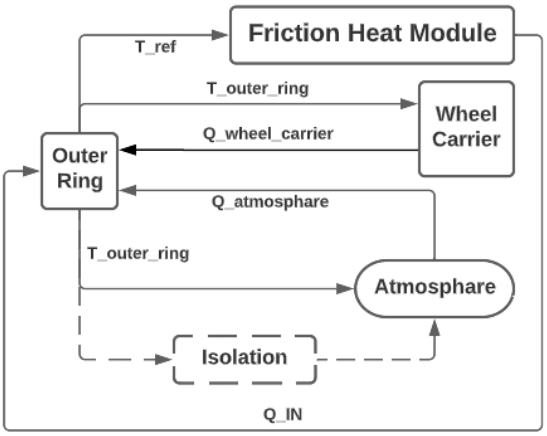

Figure 4. Heat distribution from the outer ring with negative energy feedback

The temperature of the outer ring is the reference signal of the model and in this case, the main parameter that indicates the accuracy of the simulation results relative to the measurement data. The outer ring is only getting heat energy from the source and transfers it directly to the wheel carrier and to the atmosphere through the optional insulation or - if not used - without it. Like in the case of the brake disc and shaft, the temperature of the wheel carrier is also considered time-invariant. The generated amount of friction heat at a given time depends on the temperature of the place where it is being generated. This reference temperature is provided by the signal of the outer ring in a way that it is connected back to the heat generation module at the end of each heat transfer cycle.

The basic nature of a 1D simulation model of a physical object with a complex geometry involves necessary usage of methods by whom the model can provide adequately precise results. In order to avoid dealing with complex geometrical shapes, the parts are represented in the model as nodes with thermal connections between them. These nodes contain the value of heat capacity of the particular component with the product of m mass and c_p specific heat capacity. Additionally, the initial amount of thermal energy is known by multiplying the heat capacity with the starting T_0 temperature, as shown in Eqn. (2). [9]

$$Q_0 = c_\mathrm{p} m T_0 \tag{2}$$

Note that due to the relative small temperature differences the temperature dependence of the specific heat capacity and the heat transfer coefficients have not been taken into account. Heat transfer calculations are solely based on steady-state principles in each simulation cycle.

To guarantee that the accuracy of the heat transfer is not affected by the omission of the geometry, the components are replaced with plain walls with δ thickness calculated from the volume (V) of the part divided by the size of its connecting surface (A). The temperature of a component is interpreted to be at the centre of the wall. To model the connection between the nodes, the transition at the contact area was replaced with thermal resistances (R_th) calculated by the thickness of the equivalent wall and the thermal conductivity (λ) of the materials. This way a similar thermal resistance network can be built like the one in the work of Keiji Mizuta et al. [10]. The calculation of the thermal resistance value of two solid bodies with a shared A connecting surface is according to Eqn. (3).

$$R_\mathrm{th} = \frac{1}{2A}\left(\frac{\delta_1}{\lambda_1} + \frac{\delta_2}{\lambda_2}\right) \tag{3}$$

The resistances (R_{1-8}) at the connecting surfaces are shown in Figure 5.

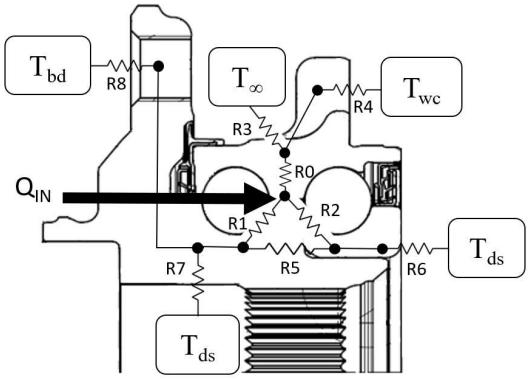

Figure 5. Schematic network of thermal resistances at the connecting surfaces

The abbreviations mean the following:

- Q_IN: friction heat generation [kJ]
- T_∞: atmosphere temperature [K]

- T_{wc}: wheel carrier temperature $[K]$
- T_{ds}: driven shaft temperature $[K]$
- T_{bd}: brake disc temperature $[K]$

The $\dot{Q}$ heat flow rate between two nodes due to their $(T_1 - T_2)$ temperature difference is defined for each time step according to *Fourier's law* for conduction in Eqn. (4) and *Newton's law of cooling* for convection in Eqn. (5).

$$\dot{Q}(t) = \frac{T_1(t) - T_2(t)}{R_{th}} \tag{4}$$

$$\dot{Q}(t) = \alpha A(T_1(t) - T_\infty) \tag{5}$$

Eqn. (4) calculates the conductive heat flow rate between two components with the usage of the R_{th} thermal resistance. In Eqn. (5), the α convective heat transfer coefficient of the fluid can only be defined by experimental measurements since it is not solely determined by the properties of the air but other influencing factors like surface geometry or the nature of the fluid flow. In heat transfer model, natural convection was modeled. The α heat transfer coefficient of the air was set to 20 W/m^2K constant as an estimated value in the case of free convection in gases. [11]

In case of using insulation around the free surface of the outer ring Eqn. (6) is used where T_1 is the surface temperature of the ring and T_∞ is the temperature of the ambient air.

$$\dot{Q}(t) = A \cdot \frac{T_1(t) - T_\infty}{\frac{\delta}{\lambda} + \frac{1}{\alpha}} \tag{6}$$

3. SIMULATION

The goal of the simulation model is to provide a fast, robust and sufficiently accurate method that can be used for estimating the energy losses of the bearing during a driving cycle.

3.1. Applied test cycle

The Worldwide Harmonized Light Vehicles Test Cycle (WLTC) and its associated Test Procedure (WLTP) is an international vehicle legislation and homologation method introduced in 2017 for passenger cars and light trucks [12]. The procedure's aim is to provide a more accurate representation of the real world driving emission and fuel consumption values than its predecessor and to make it possible to compare these values internationally. The simulations and measurements in this study use the WLTC cycle for Class 3b vehicles shown in Figure 6.

The 1800s long cycle contains four sequential ranges in ascending order by the maximum value of the speed in the particular range. The first "Low" region is meant to simulate the real world urban driving scenario while the "Medium", "High" and "Extra High" sections are respectively for the suburban, main road and highway driving scenarios [13]. The test is carried out in laboratory conditions on a chassis dynamometer in a standardised 23°C ambient temperature to ensure the procedure's repeatability.

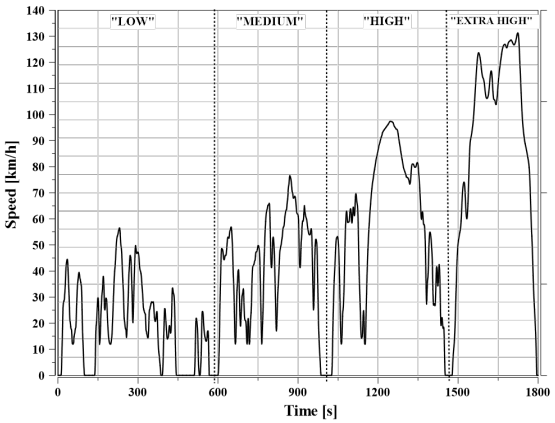

Figure 6. The vehicle speed curve used during the Class 3b WLTC

3.2. Applied validation metrics

The accuracy of the simulation model is evaluated by comparing its results to the measurement data. For that, standardised validation metrics were used which provide quantitative characteristics in addition to the qualitative assessment of the curves. The metrics use the set of prediction points (P_i) of the simulation result and the set of measured observation points (O_i) to define a single value based on which the accuracy can be classified. Both the modeled P_i and observed O_i data sets are normalised.

Many recommendations can be found in the work of Hanna et al. [14, 15] regarding the usage of statistical evaluation metrics for measuring the performance of models. A brief description of the six metrics applied in this paper is introduced in the following.

3.2.1. Hit rate (HR)

The calculation of the Hit rate (q) happens according to Eqs. (7) to (8) where the n number of P_i and O_i data point pairs are assessed whether their deviation falls into a predefined range. The range is limited by the relative uncertainty (D) and the absolute uncertainty (W) of the comparison data. [16]

$$q = \frac{1}{n}\sum_{i=1}^{n} N_i \tag{7}$$

$$N_i = \begin{cases} 1 & : \left|\frac{P_i - O_i}{O_i}\right| \le D \; or \; |P_i - O_i| \le W \\ 0 & : else \end{cases} \tag{8}$$

Assuming an ideal model means $q = 1$.

3.2.2. Factor of *n* observations (FACn)

When it comes to measure the effect of infrequent high and low O_i and P_i points, the fraction of predictions within a chosen n number as factor of observations is the most robust measure. It counts those cases when the quotient of the P_i and O_i point pairs are within a band given by a lower and upper limit that are calculated with n. Cases when one or both of O_i and P_i are outside of the W are resulting 0 value according to Eqn. (9). The calculation of the final value of $FACn$ is identical to q in Eqn. (7).

$$N_\mathrm{i} = \begin{cases} 1 & : \frac{1}{n} \leq \frac{P_\mathrm{i}}{O_\mathrm{i}} \leq n \; and \; (O_\mathrm{i}, P_\mathrm{i}) \leq W \\ 0 & : \; else \end{cases} \tag{9}$$

An ideal model would result $FACn = 1$. [16]

3.2.3. Fractional bias (FB)

With this linear measure over and under predictions can occur due to the fact that it is based on the mean bias. To solve that, false negative (FB_FN) and false positive (FB_FP) values are used to calculate the final value of FB according to Eqn. (10). The FB indicates only systematic errors.

$$FB = \frac{\sum_i (O_\mathrm{i} - P_\mathrm{i})}{0.5 \sum_i (O_\mathrm{i} + P_\mathrm{i})} = FB_\mathrm{FN} - FB_\mathrm{FP} \tag{10}$$

In case of a perfect model $FB = 0$. [16]

3.2.4. Normalised mean square error (NMSE)

Unlike the FB, the $NMSE$ metric is useful to indicate unsystematic errors. The common drawback of the two is the strong influence by the infrequent peaks of data set points. In Eqn. (11), the symbols with overline indicate the average over all points in the given data set.

$$NMSE = \overline{(O_\mathrm{i} - P_\mathrm{i})^2} / \overline{O_\mathrm{i} P_\mathrm{i}} \tag{11}$$

A perfect model would have $NMSE = 0$. [16]

3.2.5. Geometric variance (VG) and mean bias (MG)

As the previously mentioned FB the MG also measure mean bias and can be used for indicating systematic errors only. The difference is that the MG is using logarithmic scale as shown in Eqn. (12). As Chang and Hanna have mentioned [17], the logarithmic scale used at both metrics helps to provide a more accurate measure when extreme high and low values occur in the data set. Similarly to FB, MG can also be expressed as an under prediction ($MG > 1$) and an over prediction ($MG < 1$). [18]

$$MG = exp(\overline{ln(O_\mathrm{i}/P_\mathrm{i})}) \tag{12}$$

Just like the $NMSE$, the VG also can be used for both systematic and random errors according to Eqn. (13).

$$VG = exp(\overline{(ln(O_\mathrm{i}/P_\mathrm{i}))^2}) \tag{13}$$

For data values of O_i and P_i that are zero the absolute deviation W as lower limit should be used. Both $MG = 1$ and $VG = 1$ if the model is ideally perfect. [16]

4. COMPARISON WITH THE MEASUREMENTS

The prediction of the following parameters have been in focus during the simulations:

- Free surface temperature of the outer ring
- Friction power loss as heat

The temperature curves were normalised by the initial temperature of the simulation in *Kelvin*. The friction power values were normalised by the friction power of a reference bearing in *kW*.

The duration of the simulation is 1800s according to the WLTP with a sampling interval of a constant 0.1s time step. To evaluate the model results relative to the observations, reference signals had to be created. The observation data contains a measurement series of five bearings, each tested two times. As for the temperature parameter, one reference signal was built by calculating the mean of all the the ten temperature measurement data series (*'Temperature_mean_All'*). The average temperature curve of the two test curves of the bearing measurement that best fitted the model result formed the second reference curve (*'Temperature_mean_BestFit'*) for the comparison. Note, that at the start of the simulation the bearing component temperatures are set to the same value as the initial temperature during a preconditioning period. The curves are shown in Figure 7.

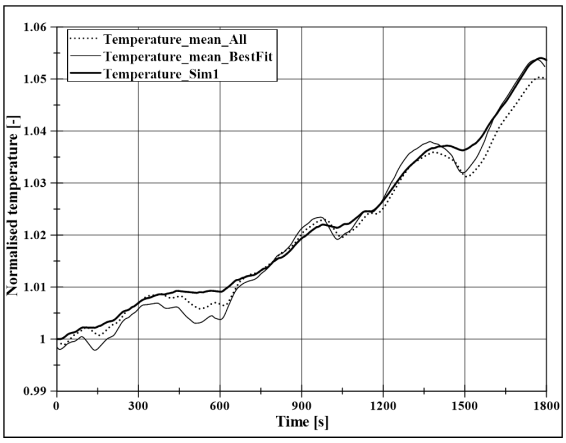

Figure 7. Comparison of the normalised temperature curves

In Figure 8. the HR is presented between the simulated temperature and the two reference signals. The error boundary is defined by the absolute error

$W = 0.006$ and the relative error $D = 0.01$. The acceptance criteria of the matching is set to $q \geq 0.66$. It can be stated based in Fig. 8 that all the points of the best fitting measurement are within the borders and it is almost the same with the mean data of all measurements. Table 1 contains the values of all the metrics used in the validation.

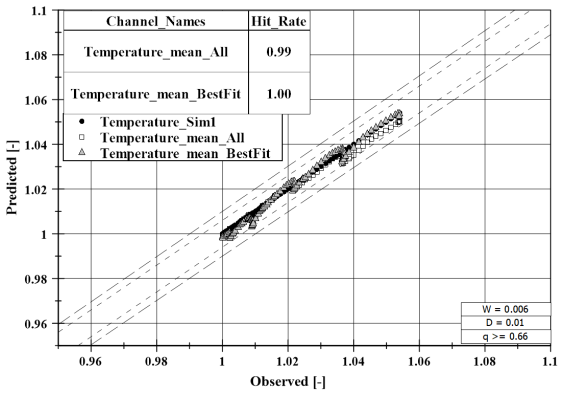

Figure 8. Temperature hit rate

Table 1. Temperature metrics values

Temperature		
Validation metrics (ideal value)	**Value**	
	Temperature mean All	**Temperature mean BestFit**
HR (1)	0.99	1.00
FB (0)	0.0014	0.0161
NMSE (0)	0.0005	0.0006
FACn (1)	0.99	1.00
MG (1)	0.99	0.98
VG (1)	1.00	1.00

It can be summarised that just like HR, all the other metrics are close to - or the same as - the ideal value, which means that the simulation approximate the observation quite well. The linearity of the model was checked with $FB \leq 0.15$ condition. For the under and over prediction analysis $0.9 \leq MG \leq 1.1$ was set for the geometric mean and also 10% deviation was allowed in the case of the geometric variance: $VG \leq 1.1$. It can be seen that in the case of $MG \leq 1$ there is a slight over prediction. The band of the $FACn$ is defined with the factor $n = 1.3$. The $NMSE$ metric is upper-limited by 0.2 ($NMSE \leq 0.2$). In Figure 9. the normalised curves are shown. The path of the friction power curve is following the WLTC's vehicle speed profile as it is pointed out in Section 2.1.

In the analysis of the friction power simulation result, the reference curves shown in Figure 10 were produced just like the ones in the case of the temperature. Because of the uncertainty of the friction power measurements the range limits were set wider for the HR by setting $W = 0.1$ and $D = 0.25$. The acceptability condition however remained the same

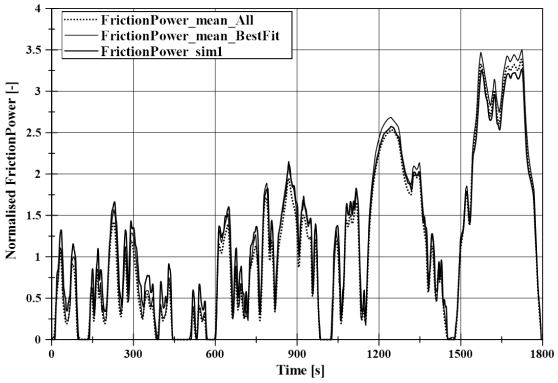

Figure 9. Comparison of the normalised friction power curves

at $q \geq 0.66$. According to the results in Table 2 only 66% of the *'mean_All'* predictions have met the conditions and 71% of the points in the *'mean_BestFit'*. The boundaries of MG, VG and FB were unchanged while the upper limit of $NMSE$ and $FACn$ was modified to 0.25 and 1.5 respectively.

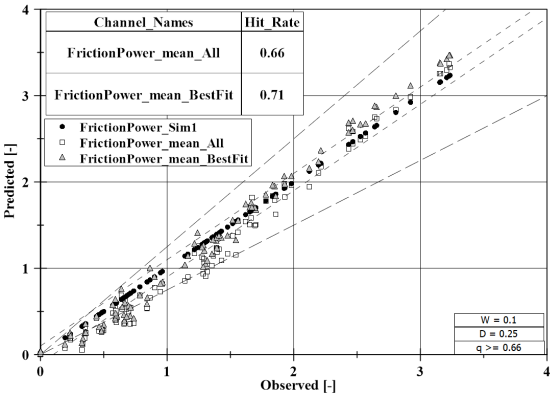

Figure 10. Friction power hit rate

Table 2. Friction Power metrics values

Friction Power		
Validation metrics (ideal value)	**Value**	
	FrictionPower mean All	**FrictionPower mean BestFit**
HR (1)	0.66	0.71
FB (0)	0.1131	0.0988
NMSE (0)	0.0214	0.0139
FACn (1)	0.79	0.84
MG (1)	0.86	0.93
VG (1)	1.19	1.16

5. EFFECT OF INSULATION

As it was mentioned in Section 2.2. the outer ring transfers heat to the wheel carrier and to the surrounding stationary air. On the other end of the assembly, the brake disc receives heat from the wheel hub. The main purpose of the simulation model was

to analyse whether the generated friction heat can be utilised substantively to decrease the rolling resistance of the bearing. As it was discussed in Section 2.1, the more heat is kept inside the bearing the more frictional losses decrease. Of course the amount of closed-in heat is upper limited by the material properties and the resulting shorter maintenance intervals. The use of an additional insulating layer on the outer surface of a part decreases the heat transfer capability. In the model this effect was interpreted in the reduction of the heat transfer coefficient of air. Beside the 23°C WLTC, the simulation was also run with -7°C to see how the colder environment affects the bearing's heat balance. Four different cases of insulation were considered in the tests that are listed here and displayed with numbers in Table 3.

- partial insulation towards the wheel carrier
- partial insulation towards the brake disc (not discussed in this paper)
- partial insulation towards the air
- partial insulation towards all three at the same time

Table 3. Heat transfer parameters for different cases of insulation

	λ **wheel carrier [W/mK]**	λ **brake disc [W/mK]**	α **air [W/m^{2}K]**
Sim 1	170	57	20
Sim 2	50	57	20
Sim 3	0.05	57	20
Sim 4	170	57	10
Sim 5	170	57	5
Sim 6	0.05	0.05	5

In the first scenario (*Sim 1*), there is no insulation on any of the components. In the case of *Sim 2* and *Sim 3* the heat transfer towards the wheel carrier is reduced with insulation in two steps. First, from 170 W/m^2K to 50 then to 0.05. Simulations 4 and 5 are the cases when the outer ring's free surface is isolated from the surrounding air represented by halving the value of α while the other parameters are changed back to their initial values. In the last scenario (*Sim 6*) the insulation is considered to affect the heat flow from the outer ring to the wheel carrier and to the air while on the other side the heat transfer from the hub to the brake disc was also decreased at the same time. The outer ring's surface temperature at each of the six insulation scenarios is displayed in Figure 11. It can be observed that the curves belonging to *Sim 2-3-4-5* are between the two extreme insulation cases when there was no insulation used (*Sim 1*) and when heat flow was blocked the most (*Sim 6*). Discussion of the separate effect of isolating the hub-brake disc connection is not part of this paper.

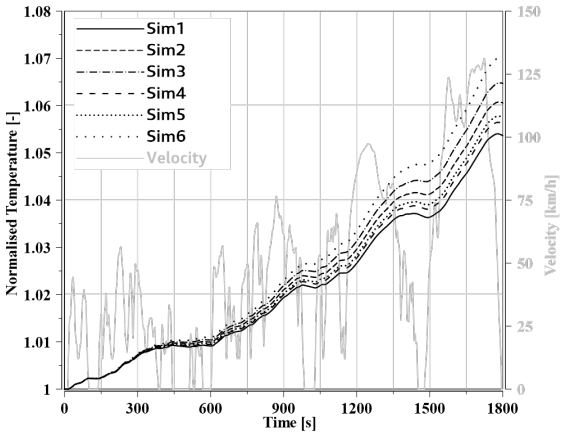

Figure 11. Normalised surface temperatures of the outer ring with different kinds of insulation. (Normalised by the starting temperature value in *Kelvin*)

As it can be observed in Fig. 11.The temperature of the outer ring is higher when more friction heat is retained by using insulation (*Sim 6*). As more heat is kept inside the system, the friction and thus the friction power is decreased. The generated friction heat energy is calculated by integrating the friction power. The effect of the insulation method on friction heat generation compared to *Sim 1* is contained in Table 4. and Table 5. The percentages of Table 4. are interpreted throughout all the WLTC tests, while the data in Table 5. is calculated only when the engine is driving the wheel.

Table 4. Change in friction heat generation with insulation compared to Sim 1. (stops & braking phases included)

	Generated Friction Heat Energy Compared to Sim 1 (stops & braking phases included)	
	WLTC 23°C	**WLTC -7°C**
Sim 2	-2.13 %	-3.08 %
Sim 3	-3.30 %	-4.79 %
Sim 4	-0.79 %	-1.15 %
Sim 5	-1.21 %	-1.75 %
Sim 6	-4.78 %	-6.96 %

Table 5. Change in friction heat generation with insulation compared to Sim 1. (driven by engine)

	Generated Friction Heat Energy Compared to Sim 1 (driven by engine)	
	WLTC 23°C	**WLTC -7°C**
Sim 2	-2.06 %	-3.01 %
Sim 3	-3.21 %	-4.67 %
Sim 4	-0.76 %	-1.11 %
Sim 5	-1.17 %	-1.70 %
Sim 6	-4.62 %	-6.76 %

6. SUMMARY

The aim of the paper was to create a 1D TMM model of a wheel bearing assembly that can be used for estimating the energy losses during a WLTC driving cycle. The 1D model contains the bearing components as thermal mass points and the thermal relations between them are governed by the well-known heat transfer equations.

The simulation results were directly compared to measurement data for validation purposes. The most important parameters were the temperature of the outer ring and the energy losses due to friction. The paper put great emphasis on the statistical evaluation of the model performance regarding its prediction capability and precision. In the following, the relation between insulations and friction heat generation were examined using two driving cycles with different ambient temperatures (23°C and -7°C).

The results of the work showed that with the usage of insulation a significant proportion of otherwise wasted friction heat energy could be utilised to decrease the rolling resistance of a given vehicle.

REFERENCES

[1] Barrand, J., and Bokar, J., 2008, "Reducing tire rolling resistance to save fuel and lower emissions", *SAE International Journal of Passenger Cars-Mechanical Systems*, Vol. 1 (2008-01-0154), pp. 9–17.

[2] Zhou, B., He, L., Zhang, S., Wang, R., Zhang, L., Li, M., Liu, Y., Zhang, S., Wu, Y., and Hao, J., 2022, "Variability of fuel consumption and CO2 emissions of a gasoline passenger car under multiple in-laboratory and on-road testing conditions", *Journal of Environmental Sciences*.

[3] Hooftman, N., Messagie, M., Van Mierlo, J., and Coosemans, T., 2018, "A review of the European passenger car regulations–Real driving emissions vs local air quality", *Renewable and Sustainable Energy Reviews*, Vol. 86, pp. 1–21.

[4] Khonsari, M. M., and Booser, E. R., 2017, *Applied tribology: bearing design and lubrication*, John Wiley & Sons.

[5] Zhaoping, T., and Jianping, S., 2011, "The contact analysis for deep groove ball bearing based on ANSYS", *Procedia Engineering*, Vol. 23, pp. 423–428.

[6] YANG, Y.-K., and JENG, M.-C., 2004, "Analysis of Viscosity Interaction and Heat Transfer on the Dual Conical-Cylindrical Bearing©", *Tribology transactions*, Vol. 47 (1), pp. 77–85.

[7] Takabi, J., and Khonsari, M., 2013, "Experimental testing and thermal analysis of ball bearings", *Tribology international*, Vol. 60, pp. 93–103.

[8] Kovalenko, P., 2021, "Heat Transfer on Wheel-Brake System at Critical Thermal Conditions", Ph.D. thesis, Georgia Institute of Technology.

[9] Flouros, M., 2006, "Correlations for heat generation and outer ring temperature of high speed and highly loaded ball bearings in an aeroengine", *Aerospace Science and Technology*, Vol. 10 (7), pp. 611–617.

[10] Mizuta, K., Inoue, T., Takahashi, Y., Huang, S., Ueda, K., and Omokawa, H., 2003, "Heat transfer characteristics between inner and outer rings of an angular ball bearing", *Heat Transfer—Asian Research: Co-sponsored by the Society of Chemical Engineers of Japan and the Heat Transfer Division of ASME*, Vol. 32 (1), pp. 42–57.

[11] Stephan, P., Kabelac, S., Kind, M., Martin, H., Mewes, D., and Schaber, K., 2010, "B1 Fundamentals of Heat Transfer", *VDI Heat Atlas*, pp. 15–30.

[12] Pavlovic, J., Marotta, A., and Ciuffo, B., 2016, "CO2 emissions and energy demands of vehicles tested under the NEDC and the new WLTP type approval test procedures", *Applied Energy*, Vol. 177, pp. 661–670.

[13] Tutuianu, M., Bonnel, P., Ciuffo, B., Haniu, T., Ichikawa, N., Marotta, A., Pavlovic, J., and Steven, H., 2015, "Development of the World-wide harmonized Light duty Test Cycle (WLTC) and a possible pathway for its introduction in the European legislation", *Transportation research part D: transport and environment*, Vol. 40, pp. 61–75.

[14] Hanna, S. R., Chang, J., and Strimaitis, D., 1993, "Hazardous gas model evaluation with field observations", *Atmospheric Environment Part A General Topics*, Vol. 27 (15), pp. 2265–2285.

[15] Hanna, S. R., 1989, "Confidence limits for air quality model evaluations, as estimated by bootstrap and jackknife resampling methods", *Atmospheric Environment (1967)*, Vol. 23 (6), pp. 1385–1398.

[16] Schatzmann, M., Olesen, H., and Franke, J., 2010, "Model evaluation case studies: approach and results", *COST 732 report*.

[17] Chang, J. C., and Hanna, S. R., 2004, "Air quality model performance evaluation", *Meteorology and Atmospheric Physics*, Vol. 87 (1), pp. 167–196.

[18] Hanna, S. R., and Chang, J. C., 2001, "Use of the Kit Fox field data to analyze dense gas dispersion modeling issues", *Atmospheric Environment*, Vol. 35 (13), pp. 2231–2242.